Bull. Mater. Sci. (2018) 41:115
https://doi.org/10.1007/s12034-018-1632-0
© Indian Academy of Sciences

In-situ TiO_2–rGO nanocomposites for CO gas sensing

SURESH BANDI, VIKRAM HASTAK, D R PESHWE and AJEET K SRIVASTAV*
Department of Metallurgical and Materials Engineering, Visvesvaraya National Institute of Technology, Nagpur 440010, India
*Author for correspondence (srivastav.ajeet.kumar@gmail.com)

MS received 15 March 2018; accepted 13 April 2018; published online 18 August 2018

Abstract. TiO_2–reduced graphene oxide (rGO) nanocomposites were synthesized *in-situ* via hydrothermal route using graphene oxide (GO), $TiCl_3$ and ammonia solution. GO was prepared by the electrochemical exfoliation technique. The structure, phase conformation and morphology of TiO_2–rGO nanocomposite were characterized using X-ray diffraction, Fourier transform infra-red spectroscopy and scanning electron microscopy. Sensing behaviour of the TiO_2–rGO nanocomposite was examined under the 100 and 200 ppm of CO environment.

Keywords. Electrochemical exfoliation; graphene oxide; TiO_2–rGO nanocomposites; chemiresistive gas sensors; CO sensing.

1. Introduction

TiO_2 is a large-band-gap semiconductor material having polymorphs of anatase (tetragonal), rutile (tetragonal) and brukite (orthorhombic) [1,2]. The anatase phase exhibits n-type semiconducting nature and rutile is a p-type semiconductor. In case of mixture of both phases, material consisting $<75\%$ rutile behaves as n-type and becomes p-type as concentration of rutile increases [3,4]. Anatase was reported well for gas sensing applications owing to its larger electron mobility behaviour compared with rutile [5,6]. On the other hand, the higher band gap ($\sim$3.2 eV) is a limiting factor for TiO_2 in view of charge carrier mobility and room temperatures sensing. Graphene is a one-atomic-layer-thick 2D material [7]. High theoretical surface area, high intrinsic carrier mobility [8] and high thermal and electrical conductivities [9] are unique features possessed by graphene. It could be a potential candidate material for chemiresistive gas sensing. However, weak adsorption characteristics towards analyte gas molecules are a drawback [10,11]. Henceforth, functionalization of TiO_2 with graphene might surpass the limitations of both materials with their synergistic effects and show better sensing properties. The synthesis of TiO_2–reduced graphene oxide (rGO) was reported for the first time by Williams *et al* [12] through UV-assisted photocatalytic reduction technique. Since then, various routes of methods are being followed to synthesize such materials of interest in various applications, viz., photocatalysis [13–17], hydrogen generation [18,19], Li-ion batteries, dye degradation [20,21], solar energy conversion [22], chemiresistive gas sensing [23,24], bio-sensors [25], etc.

In the present work, TiO_2–rGO nanocomposite was synthesized using hydrothermal approach. Also, CO gas sensing behaviour of nanocomposite material was investigated in view of utilizing the synergistic effect of TiO_2 nanoparticles and graphene.

2. Materials and methods

2.1 *GO synthesis*

Electrochemical exfoliation was employed for the synthesis of GO [26,27]. Two graphite rods were selected for anode as well as cathode; 0.35 M H_2SO_4 was prepared to be used as the electrolyte. Anode and cathode were immersed in the electrolyte with the distance of 10 cm away from each other. The initial voltage bias of 2 V was supplied for 2 min. Later, it was ramped up to 10 V for 2 h (until complete exfoliation of anode) [27]. The exfoliated GO during the process was separated from electrolyte and cleaned several times with distilled water and ethanol. Further, the obtained GO powder was dried in an oven at 60°C for overnight.

2.2 *Synthesis of in-situ TiO_2–rGO nanocomposite*

GO of 60 mg was added to 30 ml of water. The solution was magnetically stirred for 1 h. One more solution made with $TiCl_3$ (10 ml) and aqueous NH_3 (0.1 ml) was added to the graphene oxide (GO) solution. The entire solution was magnetically stirred for 30 min. Further, it was transferred to an autoclave and heated at 180°C for 12 h. The as-synthesized product was isolated by centrifugation for 10–15 min at 5000–8000 rpm. The precipitate was washed with distilled water and ethanol several times and dried in an oven at 60°C for 5 h. Finally, the TiO_2–rGO nanocomposite powder was obtained.

A schematic representation of entire process is shown in figure 1.

2.3 *Characterization*

X-ray diffraction (XRD) pattern profiles of the GO and TiO_2–rGO composite were collected using a PANalytical X'Pert Pro Multi-Purpose Diffractometer (MPD) in Bragg-Brentano geometry equipped with an X'celerator detector with Cu-K α (λ = 1.5406 Å) radiation (45 kV, 30 mA). The measurements were carried out in 2θ range of 10–100° using step size of 0.02° with 30 s time per step. The High Score plus software (3.0 e) was used for further analysis. Fourier transform infra-red (FTIR) spectra was recorded on a Perkin Elmer Spectrum One FTIR spectrometer over the range of 500–4000 cm^{-1}. The morphological behaviour of products was observed microscopically using a scanning electron microscope (SEM JEOL 6830A).

2.4 *CO gas sensing*

The TiO_2–rGO nanocomposites were drop casted on to the inter-digitized electrode substrate. The substrate was placed in a gas sensing chamber. Electrical connections were fixed. Input voltage of 1 V was given and resultant resistance data given by the sensor were collected using an indigenously made resistance measurement unit (Sensify Technologies). CO gas was sent to the chamber with varying quantity of 100 and 200 ppm. The resultant resistance variation data were collected and plotted with respect to the time. The entire process was carried out at room temperature. The sensitivity (S) of the materials towards CO was calculated using Eq. (1):

$$S = \Delta R/R_a, \tag{1}$$

where $\Delta R = R_a - R_g$, R_a is resistance prior to CO interaction and R_g the resistance of the material with CO interaction.

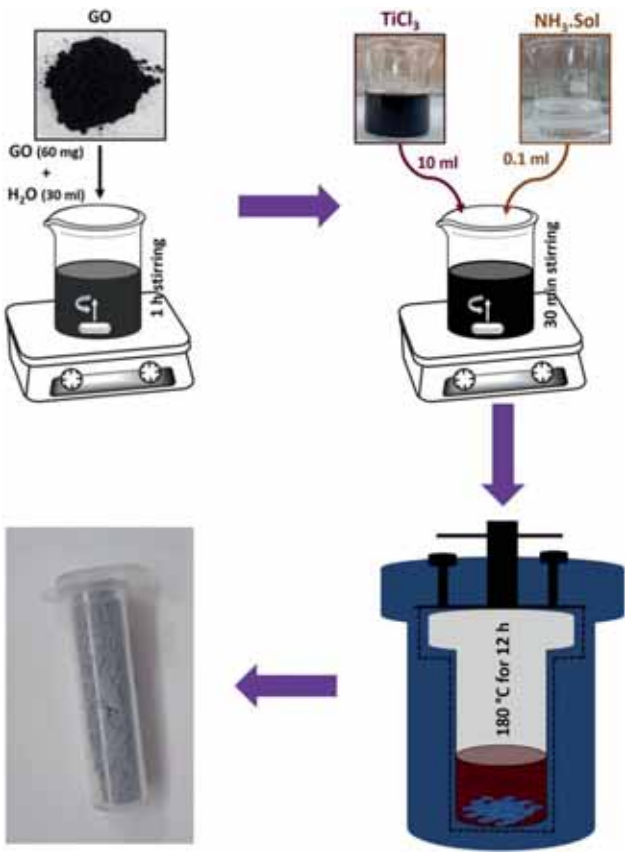

Figure 1. Schematic showing the outline of TiO_2–rGO synthesis.

3. Results and discussion

During the synthesis of TiO_2–rGO, the Ti^{3+} ions reduced GO nanosheets to rGO in the aqueous NH_3 medium. The possible chemical reactions during the process were discussed by Shen *et al* [28] as follows:

$$Ti^{3+} + GO \rightarrow TiO_2^+ + rGO \tag{2}$$

$$TiO_2^+ + H_2O \rightarrow TiO_2 + 2H^+ \tag{3}$$

The phase of TiO_2 formed in the nanocomposite was confirmed to be anatase (COD ref no: 96-900-8214).

Anatase is an n-type semiconductor material, whereas rutile (the other allotrope of TiO_2) possesses p-type semiconducting behaviour [4,29]. In general, n-type semiconductors are said to be better for gas sensing in view of conductivity, thermal stability and stability towards analyte [30]. Also, the electron mobility in anatase is significantly better than that of rutile structure due to the smaller electron effective mass and higher Fermi level of about 0.1 eV [31].

The observed XRD spectrum is shown in figure 2. The extra peaks correspond to the graphene sheets. The line profile analysis (LPA) was employed to quantify the structural parameters such as crystallite size of TiO_2 nanoparticles. The XRD pattern was fitted using a pseudo-Voigt function for the microstructural analysis. The adopted LPA considers integral breadth as a measure of peak width and universal shape factor for the peak shape variation. The instrumental broadening was removed using a silicon standard sample where the same pseudo-Voigt profile fitting function was used. The details of other profile fitting parameters have been discussed elsewhere [32,33]. In the present work, the strain contribution in the peak broadening was ignored while calculating the crystallite size of the anatase nanoparticles due to the chemical nature of the synthesis route. The single line approximation method was adopted for the crystallite size calculation using the most intense peak (0 1 1). The calculated crystallite size was 13 nm.

The FTIR spectra of TiO_2–rGO is illustrated in figure 3. The peaks at 3326 and 1626 cm^{-1} are due to O–H stretching of water molecules, which is attributed to the affinity of

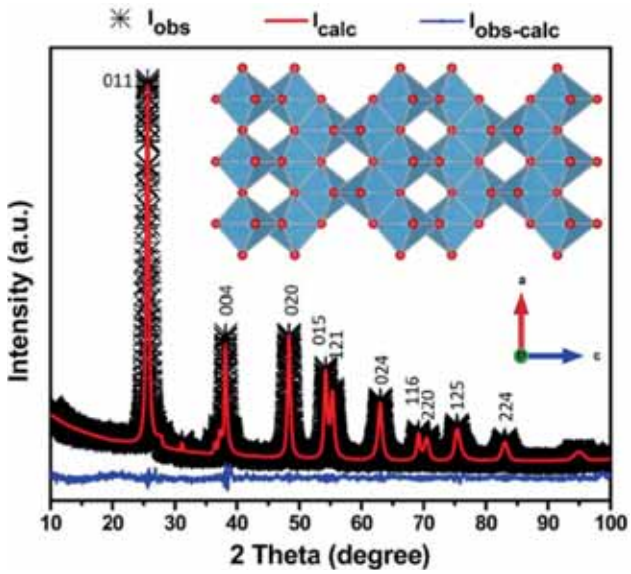

Figure 2. XRD line profile analysis of the TiO_2–rGO nanocomposite. I_{obs} is the intensity obtained from the sample, I_{calc} is the intensity of the calculated profile using the pseudo-Voigt function and $I_{obs-calc}$ is the difference between observed and the calculated profiles. The inset shows the crystallographic representation of TiO_2 (anatase) phase viewed normal to its *b*-axis.

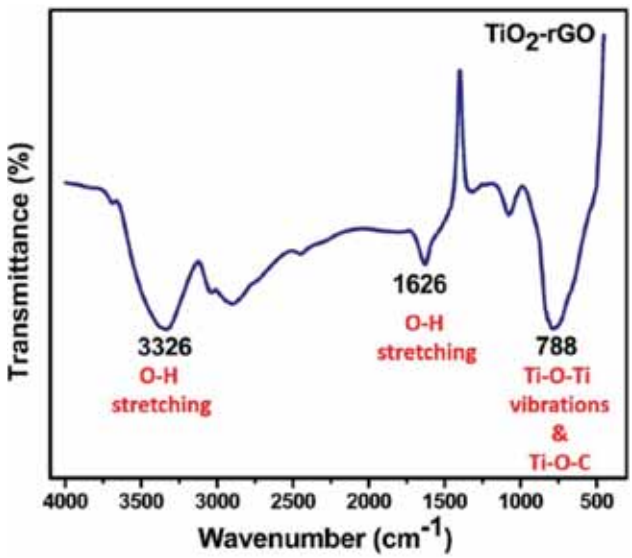

Figure 3. FTIR spectra of the TiO_2–rGO nanocomposite.

TiO_2 nanoparticles towards moisture in air [34]. The broad adsorption at low frequency appearing at 788 cm^{-1} is due to the vibrations of Ti–O–Ti bonds and the possible Ti–O–C bonds [35–37].

A SEM micrograph of the TiO_2–rGO nanocomposite is shown in figure 4. The rGO nanosheets along with TiO_2 nanoparticles are clearly evidenced in the micrograph.

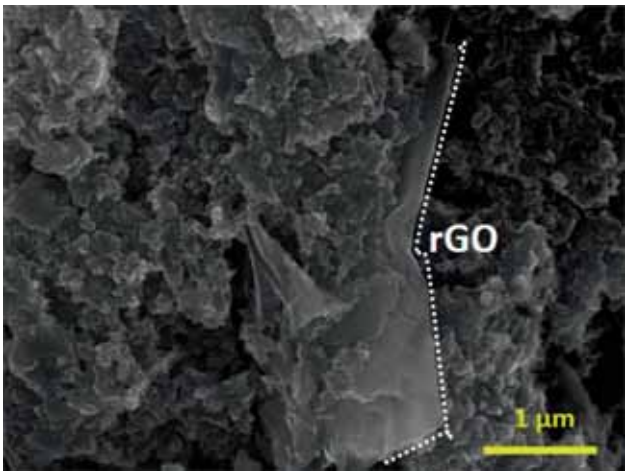

Figure 4. SEM micrograph of the TiO_2–rGO nanocomposite.

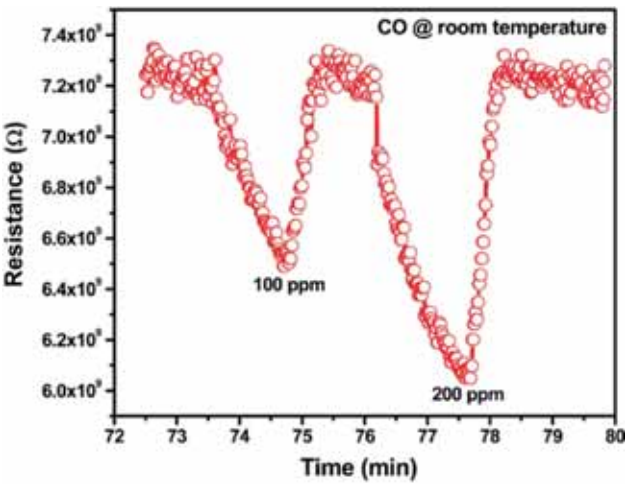

Figure 5. Sensing observation of TiO_2–rGO in 100 and 200 ppm CO environment at room temperature.

The rGO nanosheets are easily distinguishable as shown by the dotted line in figure 4.

The chemiresistive sensing behaviour of TiO_2–rGO nanocomposite in CO environment at room temperature is shown in figure 5. It was observed that the initial resistance (prior to the interaction of CO) exhibited by the material was 7.25 GΩ. Subsequent interaction of CO with TiO_2–rGO reduced its resistance immediately. This behaviour is attributed to the increase in charge carrier density in the sensing material. Being a reducing gas, CO donates electrons to the sensing material once it gets adsorbed on to the surface. The increase in electron density in n-type semiconducting TiO_2–rGO nanocomposite material led to the increased electrical conductivity. The resistance of the material was decreased to 6.5 and 6.05 GΩ due to the interaction of 100 ppm and 200 ppm of CO, respectively. Also, the resistance of material reached the initial value on removal of CO. The sensitivity of the TiO_2–rGO nanocomposite material towards 100 and

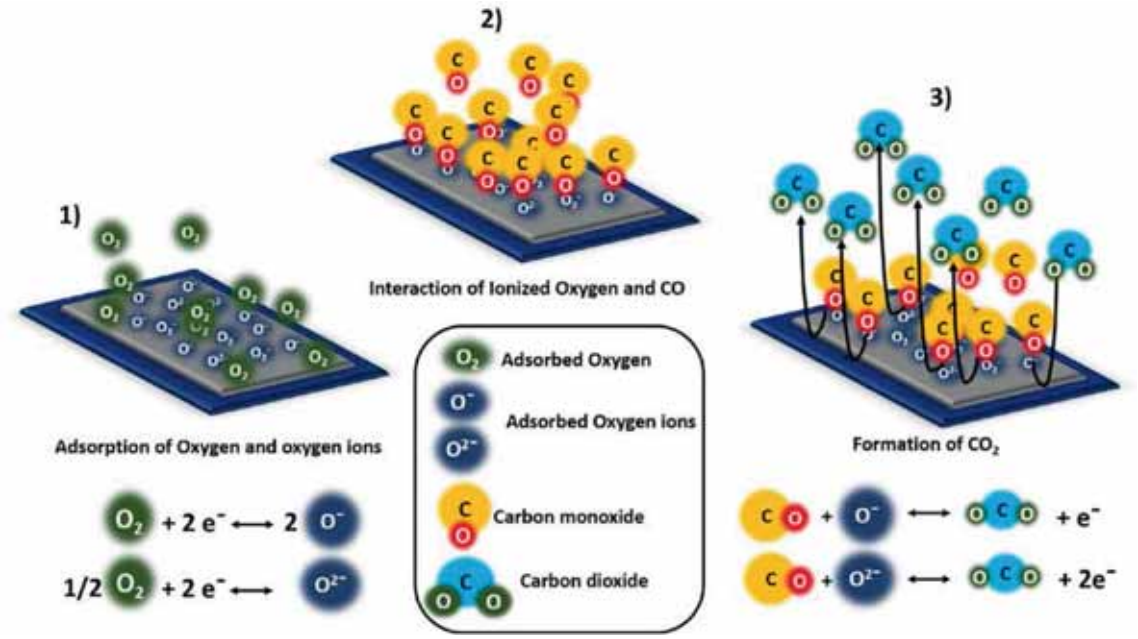

Figure 6. Schematic for CO sensing mechanism in rGO–TiO_2 nanocomposite: (1) adsorption of oxygen on to the sensing layer and subsequent ionization to O^-, O^{2-} and O_2^-, (2) interaction of CO on the sensing layer where ionized oxygen was adsorbed already and (3) reaction between CO and ionized oxygen, which results in the formation of CO_2.

Table 1. Comparison of the CO gas sensing from literature with this study.

Material	Temperature (°C)	Detection range (ppm)	Sensitivity	Ref.
SnO_2–CuO	180	100	$\sim 9.2^b$	[40]
SnO_2–graphene	150	30	0.87^a	[41]
SnO_2	150	30	0.5^a	[41]
rGO–TiO_2:Nb (5%)	380	100	$\sim 3^b$	[42]
TiO_2:Nb	380	100	1^b	[42]
Au-functionalized ZnO nanowires	RT	100	0.05^a	[43]
Shell-shaped carbon nanoparticles	RT	100	0.08^a	[44]
Pt-doped ZnO–CuO	RT	100	1.25^b	[45]
Au–SnO_2 core–shell nanoparticles	RT	1000	0.39^a	[46]
NiO	RT	100	1.12^b	[47]
NiO–graphene	RT	100	1.2^b	[47]
TiO_2–rGO nanocomposite	RT	200	0.1^a, 1.12^b	Present work
TiO_2–rGO nanocomposite	RT	200	0.16^a, 1.6^b	Present work

$a = \Delta R/R_{air}$; $b = R_{air}/R_{gas}$; RT = room temperature.

200 ppm CO was calculated using Eq. (1). The observed sensitivity for 100 and 200 ppm CO was 0.1 and 0.16, respectively.

The possible mechanism for sensing of CO can be explained as follows. Prior to the CO interaction with sensing material, the oxygen in the atmosphere adsorbs on to the surface. Due to the higher electronegativity, the adsorbed oxygen extracts the electrons from conduction band and ionizes to O^-, O^{2-} and O_2^-. When CO comes into contact, it reacts with ionized oxygen. CO_2 and excess electrons will be released as reaction products. CO_2 flies away and the excess electrons help in increasing the conductivity of material [38,39]. A schematic representation of the mechanism is shown in figure 6. The rGO contributes to increase the overall conductivity of the materials and helps the sensor to work at room temperature [23].

To explain the standpoint of present work in view of sensing ability, a few earlier CO sensing reports are compared in table 1. Our material exhibited nearly equal or better performance than that of the materials tested at room temperature.

The sensing abilities are reported to be better for sensing tests conducted at higher temperatures. However, the former comparison cannot be taken into consideration as the sensing measurement conditions are not the same.

4. Conclusion

In-situ synthesis of TiO_2–rGO nanocomposite was realized using the hydrothermal approach. The crystallite size of anatase nanoparticles was calculated as 13 nm using the XRD line profile analysis. The GO sheets were evidenced in the nanocomposite having clean interface with the nanoparticles. The chemiresistive CO gas sensing behaviour of the TiO_2–rGO nanocomposite was investigated with varying CO concentration at room temperature. Decreased resistance (increased conductivity) was observed for the nanocomposite material as compared with the air atmosphere. This was attributed to the increased charge carrier density due to adsorbed CO at the nanocomposite material surfaces. The study suggests that the synergistic effect of TiO_2 nanoparticles and graphene in their nanocomposite materials should be explored further to understand their room temperature CO gas sensing behaviour. Also, the TiO_2–rGO nanocomposite material can be tried for other gases as a chemiresistive sensing material.

Acknowledgements

A K Srivastav gratefully acknowledges the financial support from DST-SERB under the early career research award (ECR/2016/001081). Also, the authors are thankful to Prof S S Umare (Department of Chemistry, VNIT Nagpur) for extending the lab facility to perform the synthesis work and Mr S L Gadge (Department of Metallurgical and Materials Engineering, VNIT Nagpur) for his constant support and motivation for the work.

References

[1] Diebold U 2003 *Surf. Sci. Rep.* **48** 53
[2] Liu Y, Tian L, Tan X *et al* 2017 *Sci. Bull.* **62** 431
[3] Al-Homoudi I A, Thakur J S and Naik R *et al* 2007 *Appl. Surf. Sci.* **253** 8607
[4] Savage N O, Akbar S A and Dutta P K 2001 *Sens. Actuator B Chem.* **72** 239
[5] Akbar S A and Younkman L B 1997 *J. Electrochem. Soc.* **144** 1750
[6] Tang H, Prasad K, Sanjines R and Levy F 1995 *Sens. Actuator B Chem.* **26** 71
[7] Zhu Y, Murali S, Cai W *et al* 2010 *Adv. Mater.* **22** 3906
[8] Morozov S V, Novoselov K S, Katsnelson M I *et al* 2008 *Phys. Rev. Lett.* **100** 11
[9] Balandin A A, Ghosh S, Bao W *et al* 2008 *Nano Lett.* **8** 902
[10] Abideen Z U, Katoch A, Kim J H *et al* 2015 *Sens. Actuator B Chem.* **221** 1499
[11] Guo L, Kou X, Ding M *et al* 2017 *Sens. Actuator B Chem.* **244** 233
[12] Williams G, Seger B and Kamat P V 2008 *ACS Nano* **2** 1487
[13] Zhang Y, Hou X, Sun T and Zhao X 2017 *Ceram. Int.* **43** 1150
[14] Liu W, Cai J, Ding Z and Li Z 2015 *Appl. Catal. B Environ.* **174** 421
[15] Xing H, Wen W and Wu J-M 2016 *RSC Adv*. **6** 94092
[16] Sohail M, Xue H, Jiao Q *et al* 2017 *Mater. Res. Bull.* **90** 125
[17] Gu L, Wang J, Cheng H *et al* 2013 *ACS Appl. Mater. Interfaces* **5** 3085
[18] Gupta B and Melvin A A 2017 *Renew. Sustain. Energy. Rev.* **76** 1384
[19] Fan W, Lai Q, Zhang Q and Wang Y 2011 *J. Phys. Chem. C* **115** 10694
[20] Gunnagol R M and Rabinal H K 2018 *Chem. Sel.* **3** 2578
[21] Minella M, Versaci D, Casino S *et al* 2017 *Electrochim. Acta* **230** 132
[22] Yang Y, Jin Q, Mao D *et al* 2017 *Adv. Mater.* **29** 1604795
[23] Li X, Zhao Y, Wang X *et al* 2016 *Sens. Actuator B Chem.* **230** 330
[24] Acharyya D, Bhattacharyya P and Member S 2016 *IEEE Electron Device Lett.* **37** 656
[25] Solanki P R, Srivastava S, Ali M A, Srivastava K, Srivastava A and Malhotra B D 2014 *RSC Adv.* **4** 60386
[26] Yu P, Lowe S E, Simon G P and Zhong Y L 2015 *Curr. Opin. Colloid. Interface Sci.* **20** 329
[27] Ambrosi A and Pumera M 2016 *Chem. Eur. J.* **22** 153
[28] Shen Q, Zhou S, Zhao X *et al* 2012 *Anal. Methods* **4** 619
[29] Savage N, Chwieroth B, Ginwalla A *et al* 2001 *Sens. Actuator B Chem.* **79** 17
[30] Korotcenkov G 2007 *Mater. Sci. Eng. B* **139** 1
[31] Maruska H P and Ghosh A K 1978 *Sol. Energy* **20** 443
[32] Langford J I 1992 *NIST Special Publicaiton* **846** 110
[33] Srivastav A K, Panindre A M and Murty B S 2013 *Trans. Indian Inst. Met.* **66** 409
[34] Yu J G, Yu H-G, Cheng B *et al* 2003 *J. Phys. Chem. B* **107** 13871
[35] Wang P, Wang J, Wang X *et al* 2013 *Appl. Catal. B Environ.* **132** 452
[36] Hai G, Huang J, Cao L *et al* 2017 *J. Alloys Compd.* **690** 239
[37] Ye Z, Tai H, Xie T *et al* 2016 *Mater. Lett.* **165** 127
[38] Comini E, Guidi V, Frigeri C *et al* 2001 *Sens. Actuator B Chem.* **77** 16
[39] Ruiz A, Dezanneau G, Arbiol J *et al* 2003 *Thin Solid Films* **436** 90
[40] Kumar A, Sanger A, Kumar A and Chandra R 2016 *RSC Adv.* **6** 47178
[41] Debataraja A, Muchtar AR, Luh N *et al* 2017 *IEEE. Sens. J.* **17** 82978
[42] Liang F, Chen S, Xie W and Zou C 2018 *J. Phys. Chem. Solids* **114** 195
[43] Joshi R K, Hu Q, Alvi F *et al* 2009 *J. Phys. Chem. C* **113** 16199
[44] Kim D, Pikhitsa P V, Yang H and Choi M 2011 *Nanotechnology* **22** 485501
[45] Yu M R, Wu R J and Chavali M 2011 *Sens. Actuator B Chem.* **153** 321
[46] Yu Y T and Dutta P 2011 *Sens. Actuator B Chem.* **157** 444
[47] Khaleed A A, Bello A, Dangbegnon J K *et al* 2017 *J. Mater. Sci.* **52** 2035